Acta Biomaterialia 128 (2021) 370–383

Contents lists available at ScienceDirect

Acta Biomaterialia

journal homepage: www.elsevier.com/locate/actbio

Full length article

Hydration-induced reversible deformation of the pine cone

Haocheng Quan[a], Arnaud Pirosa[b], Wen Yang[c,*], Robert O. Ritchie[d], Marc A. Meyers[a,b,c,*]

[a] Materials Science and Engineering Program, University of California, San Diego, California 92093, USA
[b] Department of Mechanical and Aerospace Engineering, University of California, San Diego, California 92093, USA
[c] Department of NanoEngineering, University of California, San Diego, California 92093, USA
[d] Department of Materials Science and Engineering, University of California, Berkeley, California 94720, USA

ARTICLE INFO

Article history:
Received 4 November 2020
Revised 24 April 2021
Accepted 26 April 2021
Available online 5 May 2021

Key words:
Pine cone
Hydration
Gradient materials
Actuation

ABSTRACT

The scales of pine cones undergo reversible deformation due to hydration changes in order to optimize seed dispersal. This improves the survivability of the pine. The reversible flexing of the scales is caused by two tissue layers arranged in a sandwich configuration: a layer composed of sclereid cells and a sclerenchyma layer. They expand differentially upon hydration (and contract upon dehydration) due to differences in the structure that are analyzed here for Torrey pine (*Pinustorreyana*) cones. In addition to this well-known mechanism by which the cellulose microfibrils in the scales vary their angle with the wood cell axis, we confirm the presence of a porosity gradient in the sclereid cells and calculate, using a model consisting of three layers, the stresses generated upon dehydration taking into account the effect of hydration on the elastic modulus. Our quantitative analysis reveals that this gradient structure can significantly decrease the stress concentrations due to the mismatch between the two layers, and show that this is an ingenious design to increase the interfacial toughness to improve the robustness of pine cone scales. We also show that each individual layer of sclereid cells and sclerenchyma fibers undergoes bending when hydrated separately, and suggest that the two layers operate synergistically to effect the required deformation for seed release. A synthetic bioinspired analog consisting of hydrogels with different porosities is used to confirm this principal actuation mechanism. These findings may inspire the materials science and mechanical engineering communities to develop more robust, biocompatible and energy-efficient actuation systems.

Statement of significance

Some biological structures can exhibit reversible deformation enabled by water inflow and outflow of their structure. We analyse the reversible motion of pine cone scales. The dehydration produces their flexure and opening, resulting in the release of seeds and their dispersal, when conditions are right. This process is reversible, and rehydration of the pine cone recloses the scales. The processes of flexing and straightening are governed by shrinking and swelling which are directed by differences in the arrangement of cellulose microfibrils in a bilayer construct. We demonstrate that the scales are more complex than a simple bilayer structure and that they actually have gradients, which significantly reduce the internal stresses and ensure their integrity. We analyse the process of opening and closing of the scales for a gradient structure in the Torrey pine cone using a simple idealized trilayer model. The results demonstrate a significant decrease in internal stresses produced by the gradient structure. Using the lessons learned from the pine cone, we produce a bilayer junction using hydrogels with different porosities which exhibit the same reversible bending response.

* Corresponding authors at: Materials Science and Engineering Program, University of California, San Diego, California 92093, USA.
E-mail addresses: wey005@eng.ucsd.edu (W. Yang), mameyers@eng.ucsd.edu (M.A. Meyers).

https://doi.org/10.1016/j.actbio.2021.04.049
1742-7061/

1. Introduction

Multi-functionality is a distinct characteristic of biological materials [1]. Compared to many structural materials that are simply load-carrying, many tissues in plants and animals can perform additional functions, such as responding to external stimuli in a prescribed fashion [2–4]. These can be heat, light, electricity, hydration, or external stress; in response to them, such natural tissues can change their intrinsic properties such as their morphology, color, transparency or mechanical properties.

This is a particularly important strategy adopted by various members of the plant kingdom to ensure their survival. One might think that plants lack mobility, but if a time-lapse video is taken, the botanical world is as vibrant as animals. Taking advantage of the seasonal or diurnal humidity changes, many plant species generate a simple and controllable hydration-induced movement to improve the survivability of their seeds [2,5–7]. One prevailing strategy is the ability of self-burial for the seeds. Wild wheat [8] and the Musky Heron's bill [9,10] are two representatives which can actuate their seed awns in reversible bending or coiling movements upon the diurnal cycle of humidity to propel them into the soil and increase their probability of germination. Another approach to enhance the survivability of seeds is releasing or dispersing them when conditions are most favorable. For instance, the ice plant inhabits arid or semi-arid areas; its seed capsules only open to release seeds when the relative humidity in the environment is sufficient for their survival [11]. Pine cones adopt an opposite strategy since their primary goal is to disperse their seeds to a broader range [12]. In rainy days, the weather is not favorable for seed dispersal and so the cones are closed to protect them. Only in the dry and windy season, dehydration drives the pine cone to open its scales and the seeds are released and carried by wind to travel for long distances. Some of the pine cones have samaras, *i.e.*, propeller-shaped seeds that are dispersed to further distances.

Since pine trees inhabit most continents, the opening mechanisms of their cones has attracted considerable interest and been studied for over sixty years [12]. The current understanding is that their hydration-induced reversible opening and closure are governed by a bi-layered structure in the cone scale [12–18]. In the outer layer, which is composed of sclerenchyma fibers, the cellulose microfibrils wind around the cell walls, making a small winding angle with the cell long axis, and thus restraining the tissue from swelling upon hydration. By contrast, the sclereid cells in the inner layer make a large microfibril angle, enabling a more significant hygroscopic swelling strain in this layer. The swelling strain mismatch in the abovementioned bi-layer model can generate reversible bending for the scales upon hydration/dehydration and confer the selective seed release mechanism for pinecones. Here we should emphasize that the 'sclereid' in the following text refers to sclereid cells and the 'sclerenchyma' refers to sclerenchyma tissue.

However, we find that the well-accepted simple bi-layer model is not complete to explain our new findings. We discovered that the individual sclereid layer and the sclerenchyma fibers can bend upon hydration independently, which is a significant supplement to previous investigations. Moreover, we identified a graded transitional porosity in each component which also contributes to the hygroscopic movement of cone scales. As a consequence, we propose, as a simplification of the gradient structure, a tri-layer model containing a transitional porous layer in the sclereids and quantitatively demonstrate that this tri-layer model can significantly reduce the stress concentration between different components compared with the previously claimed bi-layer architecture. The enhanced interfacial toughness makes the hydro-actuation of cone scale more durable; indeed, our results may bring to life new inspiration for biocompatible actuation systems.

2. Materials and methods

2.1. Pine cone

The cones were collected from Torrey pines (*Pinus torreyana*) on Torrey Pine Road (La Jolla, CA, 92037). The scales were cut from the cones using a diamond saw; all the video and images were recorded using Webcam. The sclerenchyma fibers and sclereids in each cone scale were separated by a Dremel rotary tool.

2.2. Preparation of hydrogels

Alginate was provided by FMC BioPolymer, LF10/60, USA. Acrylamide (AAm) (99+%) was purchased from Acros, USA. N,N′-Methylene bis(acrylamide) (MBAA), ammonium persulfate (APS) (>98%), N,N,N′,N′-tetramethyl-ethylenediamine (TEMED) (>99%), and calcium sulfate dihydrate (98%) were purchased from Sigma Aldrich. All materials were used as received without further treatment.

The hydrogel was synthesized based on the method proposed by Sun et al. [19] with minor modifications [20]. 1 g of alginate and 8 g of acrylamide were dissolved in 51 g of deionized water, and then mixed with 0.0048 g of MBAA and 0.02 g of APS, which are the crosslinker and thermal initiator for acrylamide, respectively. The mixture was stirred at room temperature for at least 2 h until it was homogeneous. After that, the solution was degassed in a vacuum chamber and used as Solution 1. Correspondingly, 0.02 g of TEMED, the initiator accelerator, and 0.1328 g of calcium sulfate dehydrate, the ionic crosslinker for alginate, were dissolved in 5 g of deionized water, sonicated for 2 min, and used as Solution 2. Solutions 1 and 2 were mixed rapidly and homogeneously, and then quickly poured into a customized mold with dimensions of 50 mm × 20 mm × 20 mm or 50 mm × 20 mm × 40 mm. Finally, the specimen was transferred into an oven at 53°C for 2 h, after which the polymerization was complete, and a double network hydrogel was formed.

The double network gel was removed from the mold after fabrication, and then frozen at -20°C for 24 h, or frozen under liquid nitrogen (-196°C) for 10 min; after that, the frozen samples were transferred into a freeze-dryer (Labconco freeze-dry system) for complete lyophilization, and dry microporous polymer matrices were generated. The tough double network gel was removed from the mold after fabrication, and then dried at room temperature for two days to generate complete dehydration.

2.3. Structural characterization

Micro-computed tomography (micro-CT) of the cone scales was conducted on air-dried samples in a Zeiss Versa 510 X-ray microscope (Zeiss, Germany) at the National Center for Microscopy and Imaging Research (NCMIR).

Scanning electron microscopy (SEM) characterization of pine cones and hydrogels was conducted with FEI Quanta 250 microscope (FEI, Hillsboro, OR). The pine cone samples for SEM characterization are first immersed in the 2.5% glutaraldehyde for 1 h to fix the structure and then dehydrated with an ascending series of ethanol contents (30, 50, 70, 90, 95 and 100 vol.% twice). To obtain an oblique fracture surface, the scale was immersed in liquid nitrogen for 30 s and fractured using forceps immediately upon removal. All pine cone and hydrogel samples were dried with Tousimis Autosamdri 815B (Tousimis, Rockville, MD) and then sputter coated with iridium using an Emitech K575X sputter coater (Quorum Technologies Ltd.) prior to observation.

2.4. Mechanical testing

Microhardness tests were performed on the polished cross-section of pine cone scales, using a LECO M-400-H1 hardness testing machine equipped with a Vickers hardness indenter at an applied load of 200 gf. The morphology of the indents was characterized by optical microscopy.

The experimental setup for actuation force testing was very simple. The basal (proximal) part of an isolated cone scale was fixed by clamps with the tip part directly contacting the load cell. With this set-up, the upward bending was generated by immersing the cone scale in a tank of hot water at ~ 80°C. The generated bending force was recorded on an Instron 3367 testing machine (Instron Corp., Norwich, MA) for 2 h.

2.5. Moisture sorption isotherm

The moisture sorption isotherm was conducted in an environmental chamber (Model: LRHS-101-LH, Shanghai Linpin Instrument Stock Co. LTD, China), with the temperature controlled at 20°C. By opening and closing the chamber door, a fluctuation in temperature within ± 1°C was generated but it returned to the preset temperature in less than 1 min. Thirty cone scales were tested in this chamber. The process of testing involved increasing the relative humidity (RH) from 30% to close to 100% in increments of 10%, and then reducing the humidity in the same manner. One should note here that precisely 100% relative humidity was not obtainable in the environment chamber. At each step, the weight of each scale was measured until it became constant. The weight measurement was conducted outside of the chamber although the samples were place back in the chamber as soon as the measurement was completed. At each RH condition, the cone scales were taken out of the chamber every 2 h and their weight measured until the variation in two successive measurements was within 0.0005 g. Then, the RH was increased by 10% and the same procedure followed. The resolution of the balance that we used was 0.0001g. As the weight at 0% RH was not able to be measured, our starting point was at 30%RH. The absorption (moisture content) was defined as follows:

$$Absorption = \frac{Weight\ of\ sample\ at\ each\ R.H. - Weight\ of\ sample\ at\ R.H.\ 0.3}{Weight\ of\ sample\ at\ R.H.\ 0.3} \times 100\% .$$

3. Results and discussion

3.1. Characterization of pine cones and reversible deformation

Fig. 1a shows the opening of a Torrey pine cone in the dry state and its closure in the wet state, respectively. Fig. 1b shows a fractured scale with its inner structure consisting of sclerenchyma fibers aligned with the longitudinal axis of the cone scale. The polished cross-section (Fig. 1c) indicates that the cone is comprised of two components: the bright part corresponds to the sclerenchyma fibers and the dark region are the sclereids. Harlow et al. [12] were the first to identify the mechanism of flexure of the scales as being determined by differences in the longitudinal expansion of the two layers. This was later confirmed by Dawson et al.[13] and Reyssat and Mahadevan [14]. This differential expansion is caused by different orientations of cellulose microfibrils, which control the hygroscopic expansion of the cells in the two layers based on the theory proposed by Fratzl et al. [21]. The sclerenchyma fibers (Fig. 1d), which are main components of the upper layer in the scales, have the cellulose microfibrils more aligned with the cells axis at a low microfibril angle (MFA) μ ~ 28.8°, as measured in Fig. 1d, thus

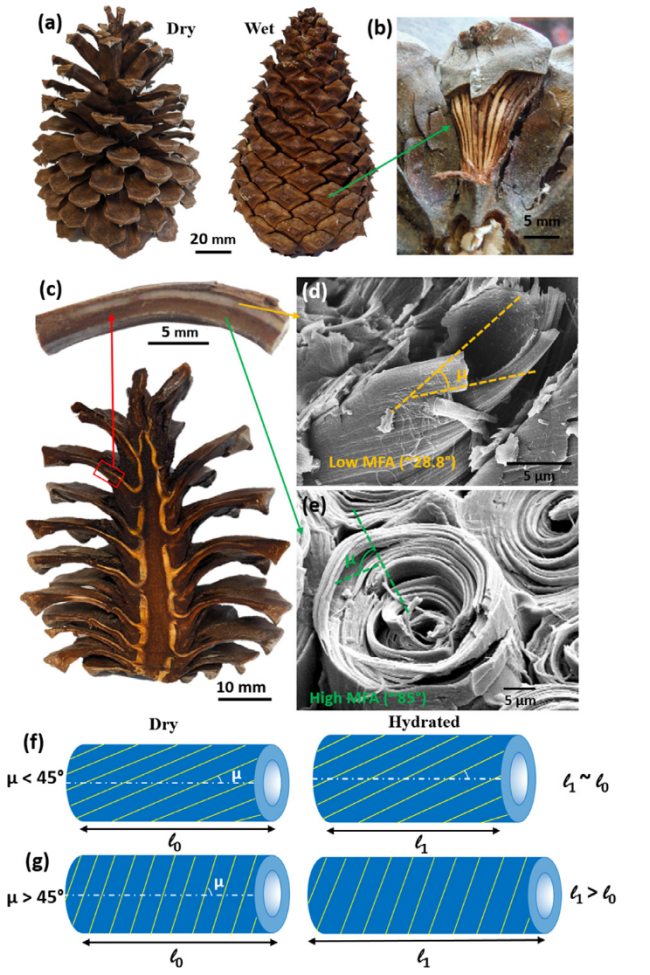

Fig. 1. Hydration-induced reversible deformation of the pine cone. (a) The pine cone in dry season opens the scales for releasing seeds and closes them in the wet state, protecting seeds. (b) A broken scale revealing sclerenchyma fibers that are covered, in the intact scale, by a sclereid layer. (c) Polished cross-section of an entire cone and a portion of isolated scale, showing double-layered inner structure. The bright upper layer is composed of sclerenchyma fibers and the dark lower region primally consists of sclereids. (d, e) SEM images of cell walls in sclerenchyma fibers and sclereids, respectively. μ is the cellulose microfibril angle (MFA). (f) small MFA (μ) between cellulose microfibrils and long cell axis of sclerenchyma fibers serve to negate any increase in the length of the fibers with hydration; (g) large MFA (μ) between cellulose microfibrils and long cell axis of sclereids generates an increase in length of the cell wall with hydration.

resisting elongation, while in the sclereid layer (Fig. 1e), the microfibrils are wound around the cell with high microfibril angle (MFA, μ ~ 85°, as measured in Fig. 1e), allowing the swelling of the matrix tissue along the long axis, which then leads to the increase in length of the wood cell [22]. Although our measured MFA values are estimates as direct interpretation from the SEM images depends on the observation angle, they are still close to the reported results in literature, such as μ ~ 30° ± 2° and 74° ± 5° measured by Dawson et al. [13]. Harlow et al. [12] measured extension strains for the sclereid layer at 0.1 and 0.37 for the fully hydrated state, whereas Reyssat and Mahadevan [14] reported a value of 0.1.

The mismatch of the swelling strain between these two components of the bi-layer structure enables these highly reversible hydration-induced movements that significantly improve the dispersal and survivability of the seeds. The mechanism is akin to that of a bi-layer thermostat with the difference that, in the latter, bending is governed by thermal expansion.

A schematic illustration of how the orientation of the cellulose microfibrils affects the longitudinal expansion of plant cell wall is

shown in Fig. 1f,g. According to the theory of Fratzl et al. [21], the stiff cellulose microfibrils undergo expansion, upon hydration, perpendicular to their longitudinal axis. If they make a small angle with the long axis of the wood cells, their swelling does not contribute to the increase in length of the latter ones. Thus, at a small microfibril angle with the cellulose microfibrils (when they are closely aligned to the long axis of the wood cell (Fig. 1f), results in lateral swelling of cell wall with no distinguishable change in its length. On the other hand, a large microfibril angle (Fig. 1g), when the microfibrils are aligned closer to the circumferential orientation, results in a constant cell diameter with hydration but now with an increasing cell wall length. Hence, the change in dimensions of a wood cell due to swelling (hydration) and shrinkage (dehydration) is a direct consequence of the winding angle of the microfibrils that comprise it.

The upward bending of pine cone upon hydration, shown in the images in Fig. S1a-c, enables the closure of the entire cone when it is immersed in water. The total angle of rotation for this isolated scale is almost 80°. Since the hygroscopic movement in pine cones is a diffusion-based process, the rate of the bending movement gradually decreases with increase of the immersion time. This is confirmed in Fig. S1d, where each colored curve represents the curvature of the cone scale at a specific time with the offset between two adjacent curves representing the change in bending angle over an interval of time. At the start of the hydration process, the curves are plotted for every 20 min and in the last 80 min, the curves are recorded for each 40 min. The results show that the variation of the curvature of the cone scale at the beginning is much faster than that during the last 2 h, confirming that the kinetics of hydration-induced bending depends on the rate of water diffusion. This is confirmed by Fig. S2 shows the variation of the ordinate of the distal end of the scale (extremity F) measured from Fig. S1, with time. The vertical ordinate increases in an approximately logarithmic manner.

Although the mechanism of bending has been identified previously [12–14], we reveal in this study two additional new aspects of this biological process. In particular, we find that the reversible hygroscopic movement of pine cones is probably not solely caused by this bi-layer structure.

The isolated layer of sclerenchyma fibers, a bundle of sclerenchyma fiber, and the sclereids were first mechanically separated, respectively shown in Fig. 2a,c,e. The three parts were independently immersed in water where we were surprised to observe that, contrary to the previous hypothesis [13], the isolated sclerenchyma and the sclereids all can deform with the uptake of water in the tissue, as shown in Fig. 2b,d,f. This interesting phenomenon consistently occurred in more than 10 sets of controlled tests, which suggests that the bi-layer structure previously proposed [12–14] is not a complete representation of the cone scale. This separate bending leads to additional synergy between the two layers, with a resultant decrease in the stresses generated. Once the structure is disintegrated and different tissues are isolated, the path of water absorption may be different from that in the whole structure, as concluded previously [16].

Micro-CT of an isolated cone scale was performed to investigate the structural organization of the sclerenchyma fibers and sclereid matrix separately. The normal view of the micro-CT scan of a cone scale is shown in Fig. 3a. However, a longitudinal cross-section of this scale, in Fig. 3b, indicates that the sclerenchyma fibers branch out and become thinner from their base (proximal) to the tip (distal) region; moreover, the density of the sclereid cells decreases with the same trend. Such a gradient in structure in different regions is confirmed in Fig. 3c,d. The close-up views of the transverse cross-section in different regions, presented in Fig. 3e,f, clearly show that the porosity of the sclereid cells has a gradient structure: the porosity (i) gradually decreases from the region close to the sclerenchyma tissue toward the dorsal surface, and (ii) gradually increases from the base of the scale to its tip. The sclerenchyma fibers also display a structural gradient. They are composed of numerous dead plant cells (Fig. 3g,h), with a non-uniform thickness varying with position among the cells; the cell walls are thinner, and the hollow tube (lumen) is larger, for the cells that adjoin the sclereid layer.

Thorough SEM characterization confirmed our findings in the CT-scan but also provided some unexpected discoveries. The gradient in porosity in the sclereid cells can be readily observed in the SEM images in Fig. 4b,c, taken from various positions marked in the overall picture in Fig. 4a. The dimension of the hollow tube in the region closer to the sclerenchyma fibers (Fig. 4c) can be seen to be larger than that in the center of sclereid layer, creating the porosity gradient indicated in Fig. 4b,c. This is consistent with our micro-CT results. In addition, the readily apparent cellulose microfibrils in the sclereids, shown in Fig. 4b, clearly manifest their circumferential orientation, which is consistent with previous reports [13]. However, contrary to the bi-layer model, the microfibril orientation in the sclerenchyma tissue (Fig. 4d) is not constant, with the microfibrils not always closely aligned with the wood cell axis [13]. Fig. 4e–g indicates that the cellulose microfibrils are not at a constant angle at different locations in the cell walls that comprise the sclerenchyma; indeed, the angle can vary even within one sclerenchyma tissue. In some regions, the microfibrils are more aligned with the axial direction of the cell (Fig. 4e) whereas in others, certain parts of the microfibrils form orthogonal pairs (Fig. 4f) or even align almost perpendicular (Fig. 4g) to the axial direction. This variation of the microfibril angles, combined with the slight porosity gradient shown in Fig. 3g, may work together to generate a gradient in hydration-induced longitudinal expansion, which confers the bending phenomenon of a sclerenchyma fiber presented in Fig. 2d. Here we have to clarify that the porosity causing the abovementioned phenomenon refers to the pores formed by the hollow cell lumen at the tissue level, as characterized in our micro-CT images, and not the pores on the wood cell walls shown in Fig. 4f.

A similar gradient architecture was also identified in the *Helichrysum bracteatum* bract. Borowska-Wykręt et al. [23] revealed that the cell wall composition at the bract hinge is not uniform. The cell wall thickness, lumen or the pore size, compactness and cellulose microfibril orientations gradually change from outer to inner surface. They demonstrated that this structural gradient is the key factor to actuate the hygroscopic movements of its bracts, which also supports our findings in the cone scales. This porous gradient in the pine cone was first observed by Song et al. [17] and Correa et al. [24]; we demonstrate here that the sclereid cells with large pore sizes act as a cushion layer between the sclerenchyma fibers and the dense sclereids, mitigating the mechanical discontinuity between these two tissues and enhancing the interfacial toughness of the whole structure.

3.2. Fabrication of a bioinspired bi-porous laminate

To establish the contribution of the porosity gradient to the mismatch in the swelling strain in each layer of pine cone scale, we fabricated double network gels with different porosities following the methodology developed by Sun et al. [19] and Sun et al. [20]. We attached them together with ethyl cyanoacrylate, forming a bi-layer porous hydrogel with different pore sizes. The initial hydrogels were prepared with same method with the different porosities were created by freeze-drying under different conditions. The macro-porous (pore size: ~50 to 100 μm) double network polymer was fabricated by freezing the gel at −20°C for 24 h prior to lyophilization, while the microporous (pore size: ~ 10 μm) double network polymer was fabricated by freezing the gel

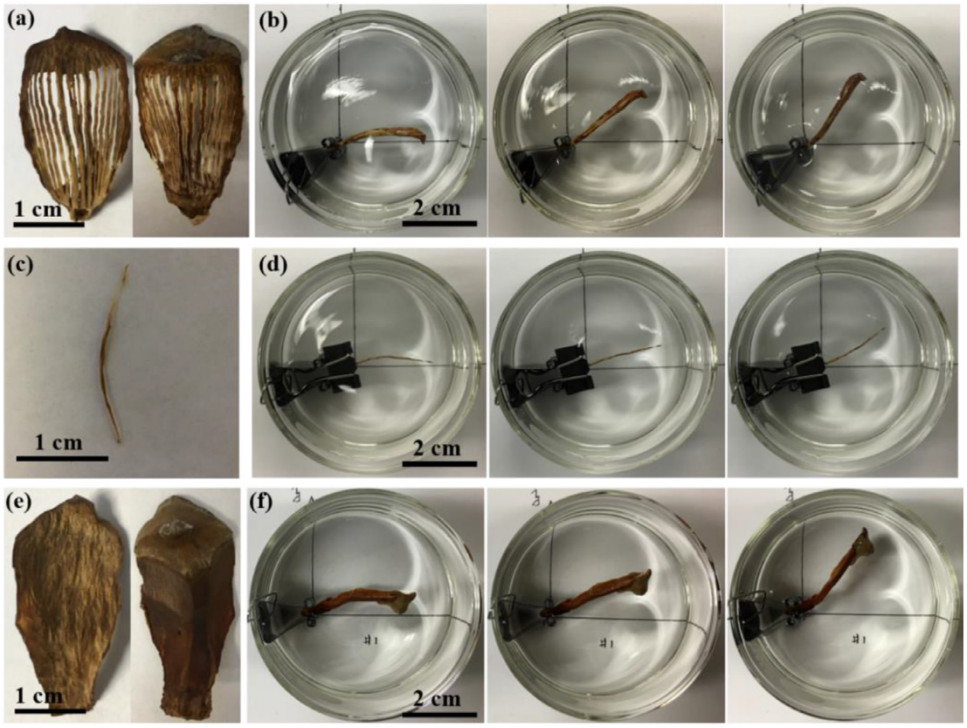

Fig. 2. The bending movement of the two components of the pine cone with hydration. (a), (c) and (e) are the images of mechanically separated sclerenchyma tissue, an isolated bundle of sclerenchyma fibers and the sclereid layer, respectively; their independent hygroscopic movements are shown in (b), (d) and (f), respectively. The time durations for (b), (d) and (f) are all 30 min.

at −196°C for 10 min prior to lyophilization. Porous structures with different pore sizes were successfully generated in the double network polymers through the freeze-drying process. The bilayer hydrogel was immersed in water overnight and from the selected time-lapse photo presented in Fig. 5, a bending deformation similar to the pine cone is observed. During a given period, the hydrogel with larger pore size has a greater ability to absorb water and the swelling strain is larger, compared to the hydrogel with smaller pore size. Based on the mismatch of swelling strains, the hydro-actuated bending deformation was achieved. This porosity induced hygroscopic expansion can be explained by Washburn equation Eq. (1) [22]. For fluid transport in a porous medium, the relationship between the amount of absorbed liquid and the material's porosity is:

$$l = \sqrt{\frac{\gamma\ r\ t\ \cos\theta}{2\eta}}, \tag{1}$$

where l is the length of the column of liquid in the capillary at the time t, η is the viscosity of the liquid, θ is the contact angle, γ is the surface energy, and r is the pore radius of the capillary. Based on this equation, the material with a larger pore size can absorb more water and generate a larger expansion in a fixed time. This is how the porosity gradient contributes to the structural expansion/contraction during the adsorption and desorption of water.

3.3. Adsorption kinetics of water

To investigate the adsorption kinetics of water in the cone tissue, the absorption isotherm of the Torrey pine cone is provided in Fig. S3. The variation in the equilibrium moisture content, *i.e.*, the weight of the increase in adsorbed water normalized by the initial tissue weight (measured at 30% RH), is plotted as a function of the relative humidity. Previously Song et al. [16] studied the path of water absorption and characterized the sequence of this absorption in different tissues in the cone scale. They demonstrated that the water-transport system among different tissues in the cone scales is highly efficient, which means that the pine cone can achieve functional movement with an economic consumption of water. Here we follow these previous research results [25–28] by attempting to analyze the water adsorption kinetics at the microlevel.

Water enters the cells and causes an increase in the volume of their walls by swelling the amorphous components (mainly hemicellulose). By varying the relative humidity at a constant temperature one can obtain the kinetics of water sorption (both adsorptions and desorption). This sorption has been studied and is known to occur in different stages. In freshly cut ("green") wood, water exists in both the lumen (inside) of the cells and in their walls. Water is attracted to the hydroxyl groups in wood and forms hydrogen bonds with them. Upon being absorbed into wood, water first enters the lumen where it stays liquid. Then, it attaches to the free hydroxyl groups of hemicelluloses and amorphous regions [25,26]. The hydroxyl groups inside the cellulose microfibrils are not accessible to water and so only the surface groups bond. This is an exothermic reaction with a decrease in enthalpy. In Fig. S3 the hysteresis upon increasing (blue line) humidity and decreasing (red line) humidity is apparent. The absorption and desorption of water are measured through the weight change in the scales. Upon increasing the relative humidity, the absorption has to restore the structure that has collapsed in the drying process. Upon decreasing the relative humidity, the water molecules find channels to escape because the swelling has created channels [26]. Thus, absorption is slower than desorption.

The first water to escape is from the cell lumens. Then, the water extant in the cell walls leaves the material. This transition is known as the fiber saturation point (FSP). For a moisture content below this point the water desorption causes shrinking. For water

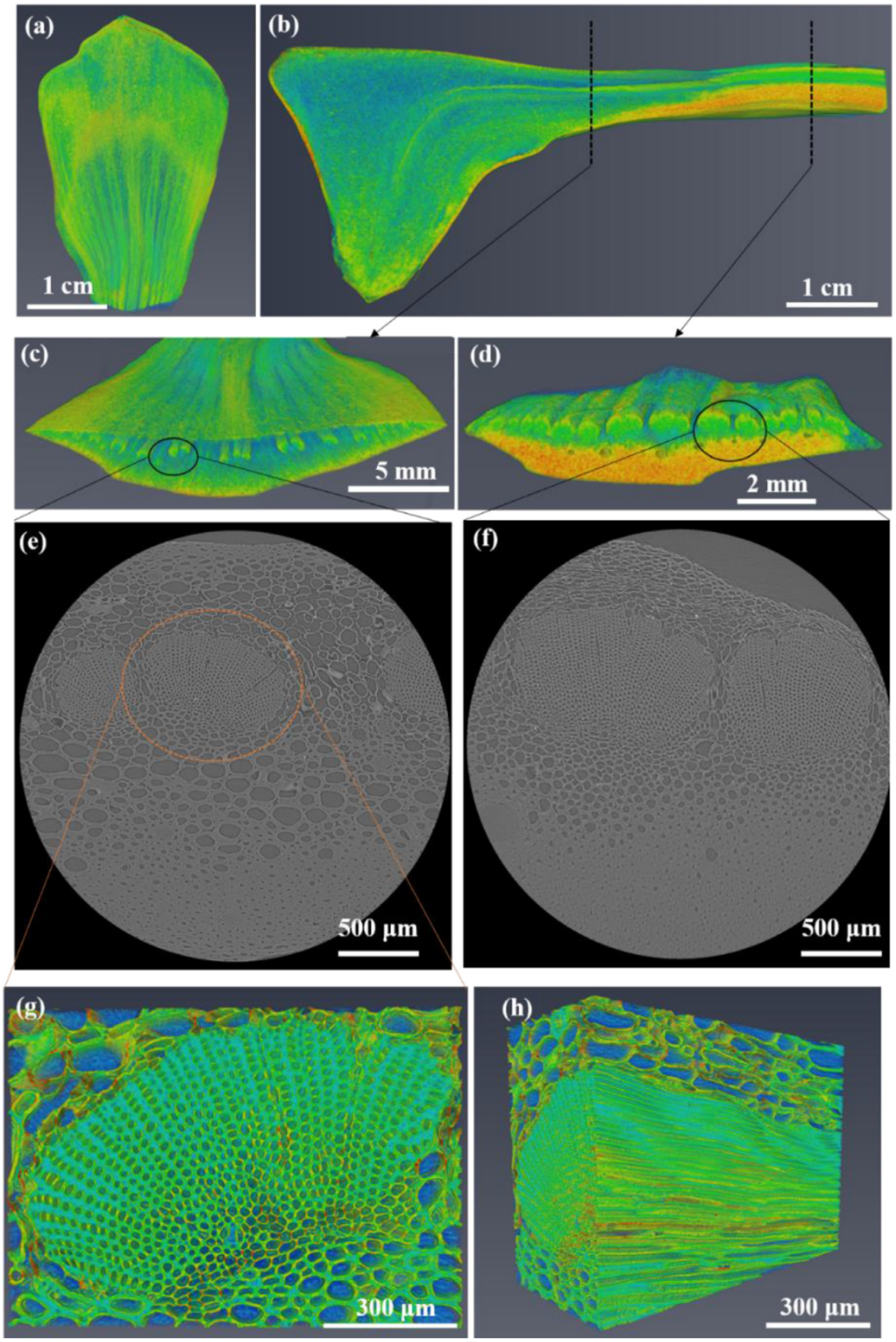

Fig. 3. Micro-computed tomography (micro-CT) of the pine cone scale. The brighter color (color closer to orange and red) indicates higher X-ray impedance, which represents higher lignification in the wood tissue. (a) Micro-CT of an isolated pine cone scale. (b) The longitudinal cross-section of the CT scan. (c,d) Transverse cross-sections of region from the distal end and proximal area, respectively. (e,f) Close-up view of (c) and (d), respectively. (g,h) Close-up view of an isolated sclerenchyma fiber and its longitudinal cross-section. Panel (a) dorsal view; (b) lateral view; (c–g) proximal view; and (h) tilted lateral view (For interpretation of the references to color in this figure legend, the reader is referred to the web version of this article.).

absorption the opposite takes place; beyond the FSP the structure swells. If the dimensions are restricted, large stresses can be generated upon water absorption. This is exemplified by the use of wooden wedges to fracture rock as long ago as in Ancient Egypt. Dry wood is inserted into the hole and when hydrated, very high stresses are generated which can fracture the rock, which has a much lower tensile than compressive strength.

3.4. Mechanical benefit of the gradient structure

Ingeniously evolved functional gradients are widely present in numerous biological materials and this design motif has already been successfully applied in many synthetic analogues to generate improved performance in comparison with discrete heterogeneities [29–35]. From a mechanistic perspective, the graded tran-

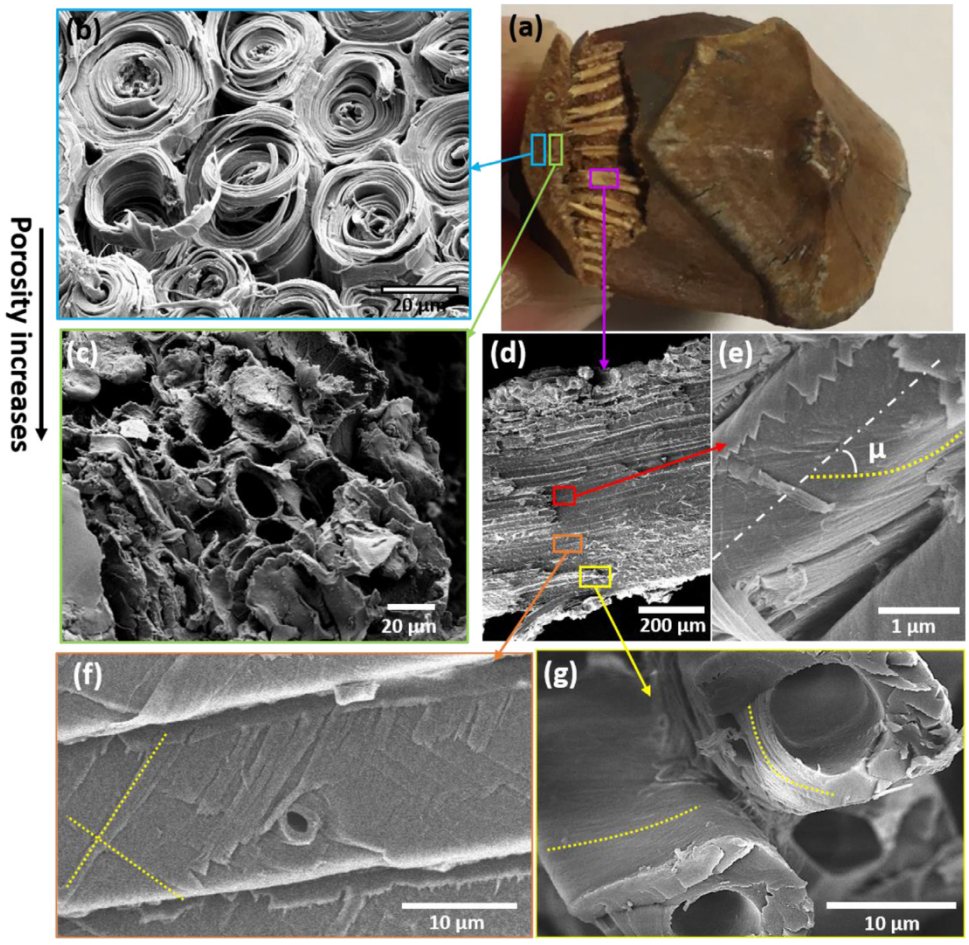

Fig. 4. SEM images of a pine cone scale. (a) Optical image showing the two components of pine cone scales: sclereid cells and sclerenchyma fibers. (b–e) SEM images of the pine cone scale. (b) and (c) are cross-sectional images of the sclereids varying in size and porosity from the bottom (b) to the region close to the sclerenchyma fiber (c). This clearly shows that the pore size in the region shown in (c) is larger than that shown in (b). (d) An isolated sclerenchyma bundle is composed of a group of fiber cells. (e–g) Fractured cross-sections of some cell walls show that the orientation of cellulose microfibrils varies in one bundle. The orientations are indicated with dotted lines. (e) The region in which the cellulose microfibrils are closely aligned with the cell axis with a small µ. (f) The cellulose microfibrils are arranged into an orthogonal pattern in some cell walls. (g) In other wood cells, the cellulose microfibrils are more perpendicular to the cell axis. Panel (a), dorsal view; (b,c) proximal view; (d-f) lateral view; and (g) proximal view.

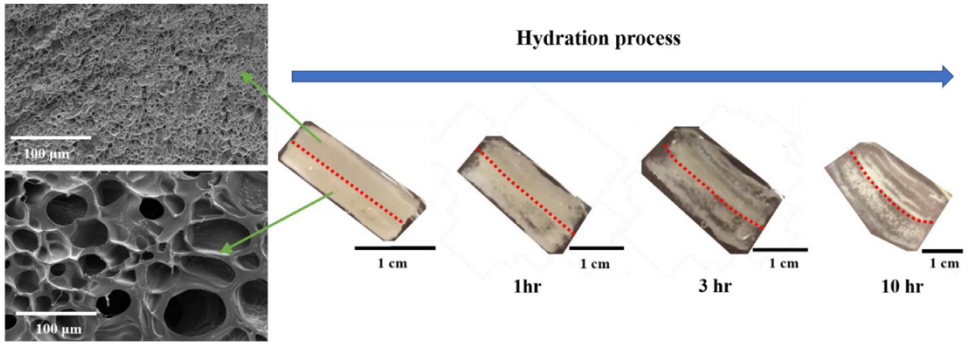

Fig. 5. Synthesized bi-layer hydrogels. SEM on left shows differences in porosity. Sequence in center and right demonstrate the contribution of porosity gradient to the hydro-actuated bending. Red dotted line marks interface between two layers (For interpretation of the references to color in this figure legend, the reader is referred to the web version of this article.).

sition can significantly reduce the stress concentration in between two distinct adjacent layers in laminated composites, which dramatically improves the interfacial toughness and increases the integrity and robustness of the whole structure [34,35]. The porosity gradient in the cone scale not only plays an important role in the hydro-actuation mechanisms that we describe above, but also benefits the mechanical performance of the scale tissue as a whole. Micro-indentation mapping (Fig. 6a) of the transverse cross-section of the cone scale shows that, for the same applied load, the indent sizes on the sclerenchyma fiber tissue (Fig. 6b) and on the denser part of the sclereids (Fig. 6c) are almost same, giving a similar hardness value (~17 HV), whereas indent sizes on the porous region of the sclereids are significantly larger, indicating a decrease in hardness to ~10 HV. To quantify

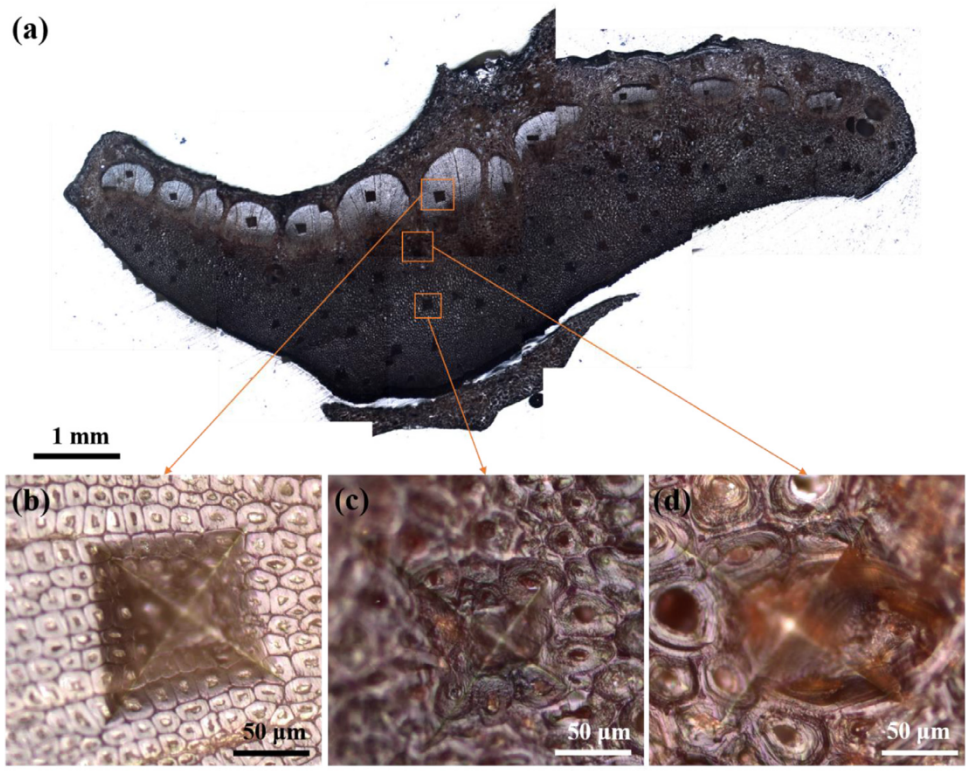

Fig. 6. Differences in hardness generated by the porosity gradient. (a) Overall view of the transverse cross-section of the indented pine cone scale sample. (b–d) Representative indentations due to a load of 200 gf on transverse cross-sections of sclerenchyma fibers, sclereids far from the sclerenchyma region and sclereids close to sclerenchyma region, respectively.

these phenomena, mechanistic modeling and analysis are provided below.

The reversible hydration of the scales is shown in the schematic representation in Fig. 7. In the hydrated condition (Fig. 7a), the scales are in the closed position and the seeds are locked in the interstices at the base. Dehydration leads to the contraction of the sclereid layer, which is considerably thicker than the sclerenchyma fiber layer. This leads to the downward bending of the scales (Fig. 7b), which serves to create open channels for the escape of the seeds. We can represent this in terms of a simple beam geometry.

An analytical solution incorporating the gradient structure is excessively complex and therefore a tri-layer approach is adopted here, as shown in Fig. 7c. This marks a progression toward a continuous change in modulus with position. The three layers are the sclerenchyma fibers, the porous sclereid layer, and the dense sclereid layer, which are designated respectively by the subscripts f, p and sc. The thickness, a, and coefficients of hygroscopic expansion, α, of these three layers are in turn designated by a_f, a_p, a_{sc} and α_f, α_p, α_{sc}. Because of differences in the hydroscopic expansion coefficients, the swelling/shrinking strains of these three layers are not same. The tight interfacial bonding enables the forces that are exerted by adjacent layers to be applied on each component. Thus, the forces applied on sclerenchyma fiber, porous sclereid and dense sclereid layers are designated as F_f, F_p and F_{sc}, respectively, and the corresponding bending moments (M) due to the difference in the hygroscopic expansion are M_f, M_p, M_{sc}. The radii of hydration-induced bending for these three layers are r_f, r_p and r_{sc}, which are approximated to r since, compared with the whole thickness of the scale, the bending is relatively small (Fig. 7d).

The porosity in the sclereid layer was quantitatively measured in three micro-CT scanned sections (marked 'slices' in Fig. 8a–c). They are similar to the micro-CT scan presented in Fig. 4e,f, from which measurements are illustrated in the inset to Fig. 8a. Figure S4 shows the three sections where measurements were made. The orange solid arrow indicates the direction of the measurement, which is from the interface between sclerenchyma fibers to the dense sclereids. The pore sizes were measured along the vertical direction at each position, as indicated by the yellow dotted lines, and the average taken. Based on the fitted curve in Fig. 8a, the pore size first rises and then gradually decreases with increasing distance from the interface between two layers (towards sclereids). The small pore size in the starting regions is due to the fact that the arrangement of sclerenchyma is not perfectly aligned and when the pores are measured along the dotted line, some pores in the sclerenchyma are included (the left-most yellow dotted line is intersected with the cross-section of sclerenchyma fibers). In the exclusive sclereid region, the graded decrease in the pore size with increasing distance from the interface is much clearer.

The relative density of porous tissue, ρ, as compared to the nonporous material with same composition, ρ_s, was calculated based on the relationship $\frac{\rho}{\rho_s} \sim (\frac{r_h}{r_c})^2$, where the r_h is the radius of the hollow tube (lumen) in the wood cell, as shown in the inset in Fig. 8b and r_c is the external radius of the cell. In our calculation, r_h is taken as one half of the pore diameter in Fig. 8a. The variation in relative density $\frac{\rho}{\rho_s}$ with distance from interface is presented in Fig. 8b. Calculation of the modulus, based on the Gibson-Ashby equation Eq. (2), can be expressed as:

$$E = E_s\left(\frac{\rho}{\rho_s}\right)^2, \tag{2}$$

where E is the Young's modulus of the porous tissue and E_s is the corresponding modulus of the solid tissue. Using this relationship, the Young's modulus of the porous layer as a function of position is plotted in Fig. 8c. It can be seen that the relative Young's modulus decreases from 0.3 at the interface with the sclerenchyma fibers

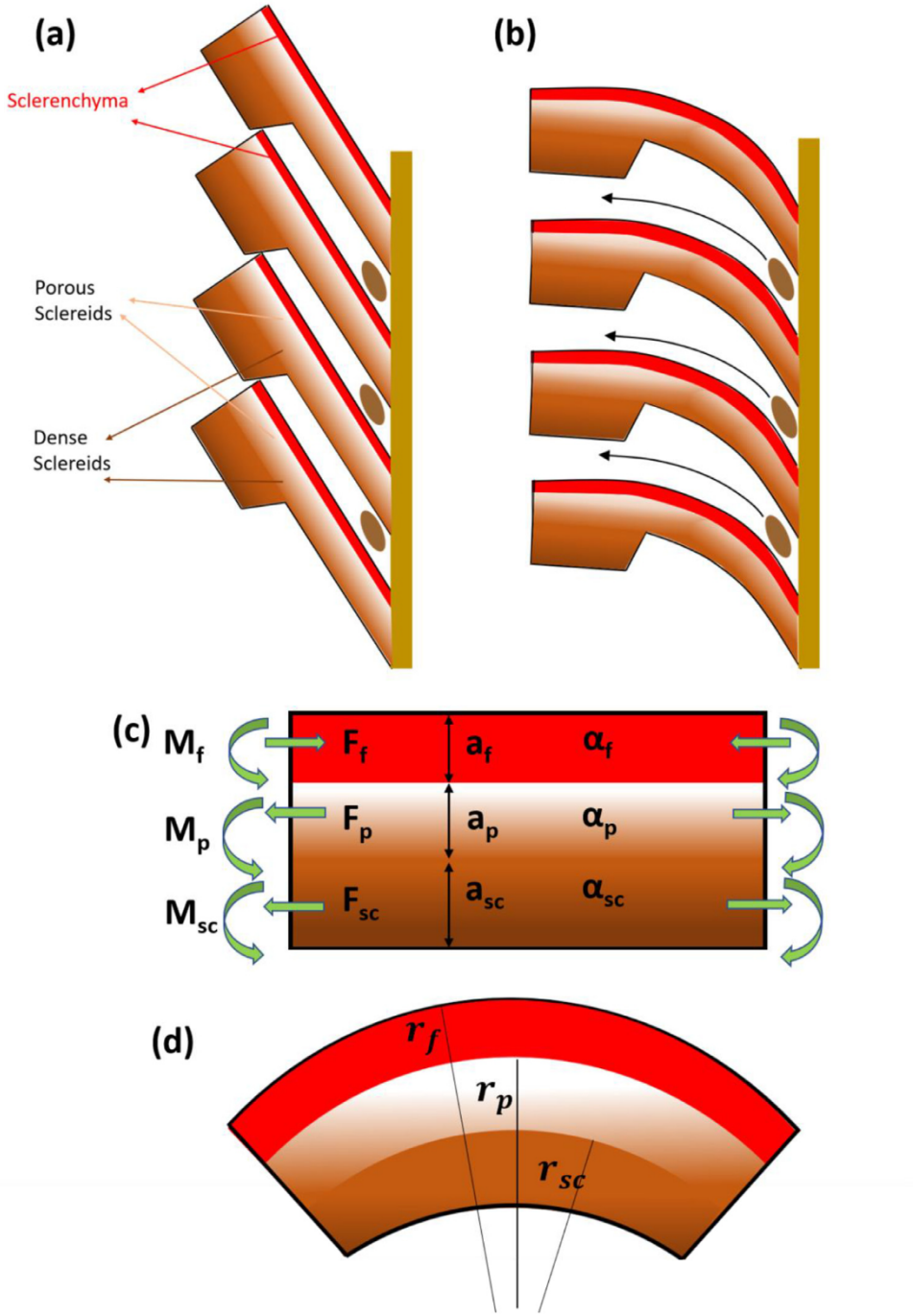

Fig. 7. Schematic rendition of reversible bending of cone scales by hydration and predicted response to hydration. (a) hydrated scales; (b) dry scales with path for seed dispersal; (c) beam configuration with a tri-layered structure for hydrated scale; (d) deformed beam configuration with radii $r_f \sim r_p \sim r_{sc} \sim r$ for a dry scale.

to below 0.1, before rising to the value of the nearly 0.6 E_s at the edge of the micrograph (Fig. 8c). In our tri-layer model, the sclereid layer is divided into two: a dense layer (with $E/E_s = 1$) and a porous layer with $E/E_s = 0.1$ (note that these are average values). This tri-layer analysis represents a departure from the previously reported bi-layer analysis, used by Reyssat and Mahadevan [14] based on the Timoshenko treatment [36]. We recognize that it is also an approximation, since porosity varies continuously, but it establishes the effect of the porous layer. Our model follows closely the one derived by Timoshenko [36] for a bimetallic thermostat by using three layers, but with the substitution of hygroscopic expansion coefficients for linear thermal expansion coefficients, the former being defined in terms of the level of hydration, h, by Eq. (3):

$$\alpha = \frac{1}{L}\frac{dL}{dh}, \tag{3}$$

where L is an arbitrary length. Note that the value of h is governed by the relative humidity, which here is assumed to vary between 0 for a dry specimen to 1 for the fully hydrated condition. We define the length L as the dimension along the long axis of the cone scale; dimensional variation along the other two directions orthogonal to the length direction was not involved in our quantitative analysis.

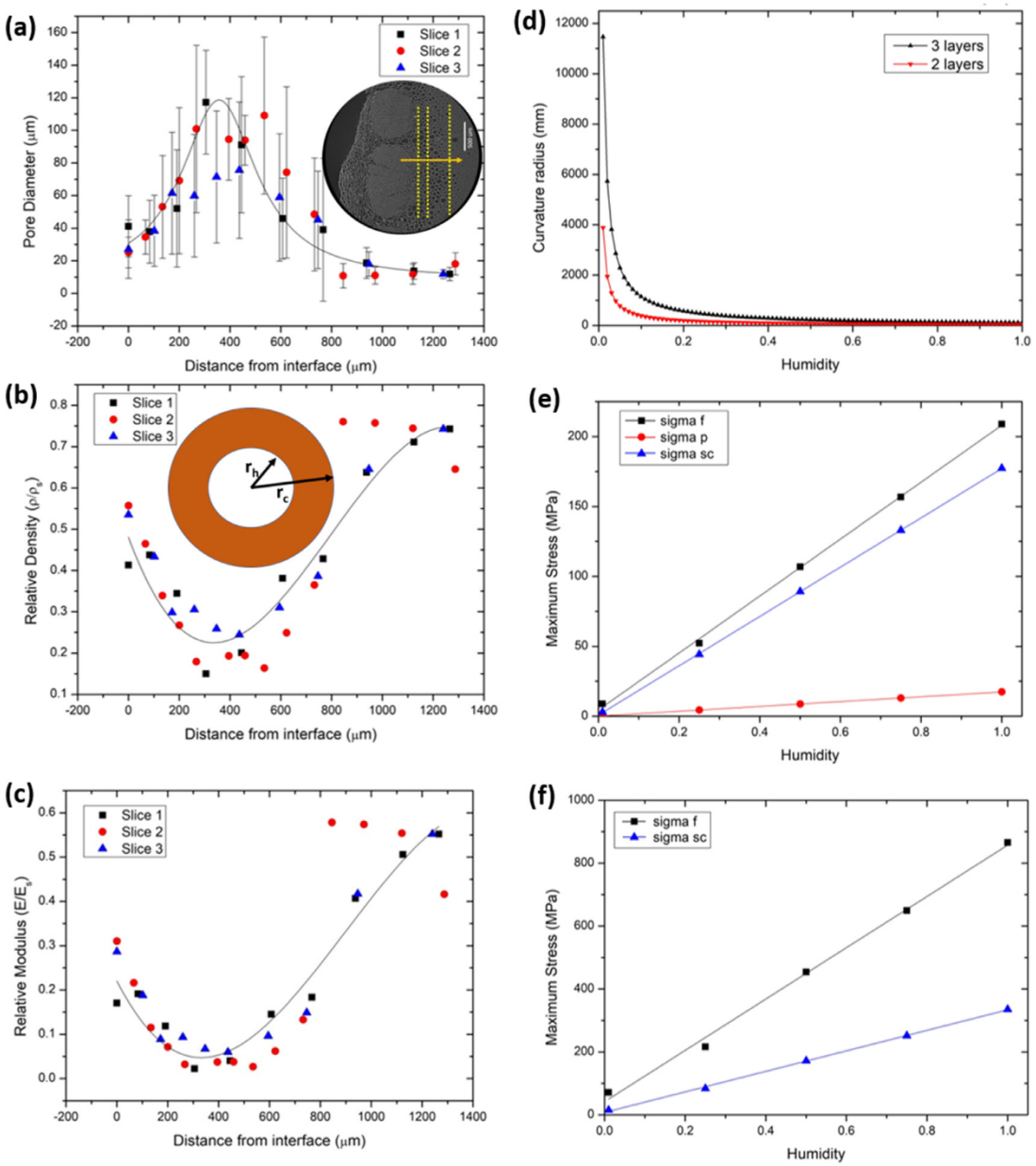

Fig. 8. Decreased interlayer stress concentration generated by the porosity gradient. (a) Measured pore diameter from the micro-CT scanned images and (b) calculated relative density in sclereid cells as a function of distance from the sclerenchyma fiber. (c) Estimated normalized Young's modulus in sclereid layer as a function of distance from the sclerenchyma fiber. (d) Radius r as a function of hydration level for bi-layer and tri-layer configurations. Upper limit (neglecting effect of hydration on Young moduli) stress distributions for (e) tri-layer and (f) bi-layer configurations. Notice that in d, e, f humidity is 1 at origin.

Based on our model in Fig. 7c, the equations of equilibrium are Eqs. (4) and (5):

$$\Sigma F = F_p + F_{sc} - F_f = 0, \tag{4}$$

$$\Sigma M = 0. \tag{5}$$

The forces are assumed to be applied to the centroids of the respective sections. Thus, the summation of the moments is shown in Eq. (6):

$$M_f + M_p + M_{sc} - F_f\left(\frac{a_f}{2} + \frac{a_p}{2}\right) - F_{sc}\left(\frac{a_{sc}}{2} + \frac{a_p}{2}\right) = 0. \tag{6}$$

The three moments can be expressed by Eq. (7):

$$M_f = \frac{E_f I_f}{r_f}; M_p = \frac{E_p I_p}{r_p};\ M_{sc} = \frac{E_{sc} I_{sc}}{r_{sc}}, \tag{7}$$

where E_f, E_p, and E_{sc} are the respective moduli for sclerenchyma fiber, porous sclereid and dense sclereid, and I_f, I_p, and I_{sc} are the corresponding moments of inertia for the three components, which are defined, for a rectangular section, per unit width, as Eq. (8):

$$I_f = \frac{a_f^3}{12};\ I_p = \frac{a_p^3}{12}\ I_{sc} = \frac{a_{sc}^3}{12}. \tag{8}$$

The strains in the sclerenchyma fibers f and the porous sclereid layer p have to be the same as that at the f-p interface; the same applies to the strains in porous p and dense sclereid sc layers and that at the p-sc interface. These are the compatibility conditions which can be expressed by Eqs. (9) and (10):

$$\text{f} - \text{p interface}: \ \alpha_f(h_1 - h_0) + \frac{F_f}{E_f a_f L} + \frac{a_f}{2r} = \alpha_p(h_1 - h_0) - \frac{F_p}{E_p a_p L} - \frac{a_p}{2r}. \tag{9}$$

$$\text{p}-\text{sc interface}: \quad \alpha_p(h_1-h_0) - \frac{F_p}{E_p a_p L} + \frac{a_p}{2r} = \alpha_{sc}(h_1-h_0) - \frac{F_{sc}}{E_{sc}a_{sc}L} - \frac{a_{sc}}{2r}. \tag{10}$$

where h_1 is the relative humidity at a given moment and h_0 is that in the initial environment: $\Delta h = h_1 - h_0$. The forces F_f, F_p, and F_{sc}, as a function of humidity, can be obtained from Eq. (4) to Eq. (10):

$$F_f = \left(\alpha_{sc}-\alpha_f\right)E_f a_f L\Delta h - F_{sc}\frac{E_f a_f L}{E_{sc}a_{sc}L} - \frac{E_f a_f L\left(a_f+2a_p+a_{sc}\right)}{2r}, \tag{11}$$

$$F_p = (\alpha_p-\alpha_{sc})E_p a_p L\Delta h + F_{sc}\frac{E_p a_p L}{E_{sc}a_{sc}L} + \frac{E_p a_p L(a_p+a_{sc})}{2r}, \tag{12}$$

$$F_{sc} = \frac{1}{A}\left[\left(\alpha_f-\alpha_{sc}\right)E_f a_f L\Delta h - \frac{E_f a_f L\left(a_f+2a_p+a_{sc}\right)}{2r} - \frac{2\sum E_i I_i}{r\left(a_f+a_p\right)}\right], \tag{13}$$

where $A = \frac{E_f a_f L}{E_{sc}a_{sc}L} - \frac{a_{sc}+a_p}{a_f+a_p}$ and $\sum E_i I_i = E_f I_f + E_p I_p + E_{sc} I_{sc}$.

The radius r as a function of humidity Eq. (14) is obtained by substituting Eqs. (11), (12) and (13) into Eq. (4), *viz*:

$$r(\Delta h) = \frac{2.\frac{\sum E_i I_i}{a_f+a_p} - \frac{\left(a_f+2a_p+a_{sc}\right)\cdot E_f a_f L-(a_p+a_{sc})E_p a_p L\cdot A\cdot B}{2} - \left(a_f+2a_p+a_{sc}\right)E_f a_f L\cdot A\cdot B}{\left[\left(\alpha_{sc}-\alpha_f\right)E_f a_f + \left(\alpha_f-\alpha_{sc}\right)E_f a_f A\cdot B + (\alpha_{sc}-\alpha_p)E_p a_p A\cdot B\right]L.\Delta h}, \tag{14}$$

where $B = [\frac{E_{sc}a_{sc}L}{(E_f a_f+E_p a_p+E_{sc}a_{sc})L}]$.

The maximum normal stresses (parallel to the scale axis) in the three layers are obtained from these forces and bending moments. They vary linearly with distance, *y*, from the centroid of each layer and are highest at the largest distance from it. These maximum and minimum normal stress values in the three layers are:

$$\sigma_f = \frac{F_f}{a_f L} \pm \frac{E_f a_f}{2r}, \tag{15}$$

$$\sigma_p = -\frac{F_p}{a_p L} \pm \frac{E_p a_p}{2r}, \tag{16}$$

$$\sigma_{sc} = -\frac{F_{sc}}{a_{sc}L} \pm \frac{E_{sc}a_{sc}}{2r}, \tag{17}$$

where the distances *y* from the centroid of each section to the outside sclerenchyma fibers are -a_f/2 to +a_f/2 for the sclerenchyma layer, -a_p/2 to +a_p/2 for the porous layer, and -a_{sc}/2 to +a_{sc}/2 for the dense sclereid layer. It should be mentioned that as the modulus values E_f, E_p, and E_{sc} are dependent on hydration, the calculated values of the stresses apply to the initial dry condition. However, Eqs. (15), (16) and (17) can be readily modified by introducing a functional dependence of the Young moduli on hydration.

Table 1 shows the values used in the calculation for the radius and stresses. These values were extracted from the dimensions of the pine cone and from the literature. They are given by Dawson et al. [13] as $\alpha_f = 0.06$ for the fiber and $\alpha_{sc} = 0.20$ for the sclereid layer. Reyssat and Mahadevan [14] give corresponding values of $\alpha_f = 0$ and $\alpha_{sc} = 0.1$. The elastic constants were taken from Dawson et al. [13] for the sclerenchyma and sclereid layer.

The tri-layer and bi-layer cases were calculated for comparison purposes. For the bi-layer case, which was analyzed by Reissat and Mahadevan [14], the total sclereid thickness was taken as the sum of the porous and solid sclereid layers in the tri-layer configuration. The radii of curvature as a function of humidity differ somewhat, the bi-layer case being more responsive to humidity changes (Fig. 8d). It is interesting to note that the stresses vary linearly with the change of humidity (Fig. 8f). This is expected since the moduli are assumed to be independent of moisture. The incorporation of the intermediate porous layer has a profound effect on the maximum stresses (Fig. 8e and f); the stress in the fibrous layer, which is the highest, is reduced from the bi-layer case to approximately one fourth in the tri-layer case. This is a very significant effect and demonstrates that the incorporation of a porous layer has a major effect on the maximum stresses. With the presence of the porous component in the sclereids that connects to the sclerenchyma fibers, the stress concentration between these two actuation components is dramatically reduced and acts as cushion layer; indeed, the porosity gradient is vital for the enhanced interfacial toughness in the whole structure, conferring an enhanced integrity and durability compared to that previously calculated for a bi-layer architecture.

Table 1
Parameters for calculation of the curvature radius r and normal stresses for a tri-layer cone scale; for bi-layer, the total sclereid layer thickness is taken as ($a_p + a_{sc}$).

Parameter	Unit	Value
a_f	mm	1.5
a_p	mm	0.8
a_{sc}	mm	1.5
E_f	GPa	4.53
E_p	GPa	0.09
E_{sc}	GPa	0.86
α_f		0.06
α_p		0.20
α_{sc}		0.20
I_f	mm^4	0.28
I_{sc}	mm^4	0.28
I_p	mm^4	0.043

As noted above, refinement of the above analysis can be made by considering that the moduli E_f, E_p, and E_{sc} are dependent on hydration. Although the calculated values of the stresses above apply to the initial dry condition, Eqs. (15), (16) and (17) can modified by introducing a functional dependence of the Young moduli on hydration. Gerhards [37] presents a plot of the relative Young's moduli as a function of moisture content for several woods along the grain, which is the same orientation as ours. Moisture Content, MC is defined as the mass of water, m_{water}, divided by the mass of the dry wood, m_{wood}. It is usually presented on a percentage basis as expressed by Eq. (18):

$$MC = \frac{m_{water}}{m_{wood}}x100 = \frac{m_{total}-m_{wood}}{m_{wood}}x100 \tag{18}$$

The maximum of MC for green wood varies from 110 to 219 for pine sapwood. The density of wood cells is ~1.54. The lower the density of wood, the greater uptake of water it can have. This is indeed a broad range. We adopted the definition of Reissat and Mahadevan [14] for humidity, f: it is zero in the dry condition and equal to 1 for water saturation (maximum).

We convert Moisture Content from Gerhards to f. Gerhards [37] presents results from MC=0 to 0.3 in their Fig. 1. The Young moduli are normalized to the value at MC equal to 12% (E_r). We use the range that is approximately linear, from MC=0.05 to MC=0.27.

This provides:

$$\frac{E}{E_r} = 1.124 - 1.2x10^{-2}MC \tag{19}$$

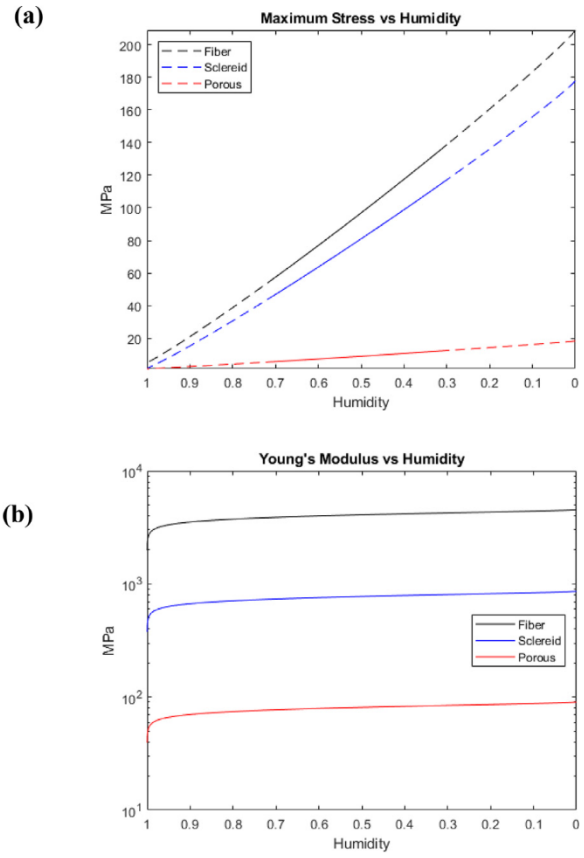

Fig. 9. Effect of relative humidity on the (a)Young's moduli and (b) stresses generated in the fiber, sclereid, and porous layers. shows a non-linear dependence of the maximum stress on humidity resulting from an assumed linear dependence of Young moduli on moisture content, extracted from the results presented by Gerhards [37] for a variety of woods along the fiber axis and by conversion of MC into h [38].

In order to convert MC into f, we have to consider the maximum value of MC for the pine cone as corresponding to f=1. E_r can be converted into E_0, the Young's modulus at h=0 (or MC=0). From Gerhards, [37] one can approximate this value as:

$$\frac{E_0}{E_r} = 1.1 \tag{20}$$

Glass et al.[38] and Glass and Zelinka [39] propose the following equation for the relationship between Moisture Content from Gerhards and Relative Humidity, h (as used by Reissat and Mahadevan [14] and in our calculations):

$$MC = 100\left[AT\left(1-\frac{T}{T_c}\right)^{B} ln(1-h)\right]^{CT^{D}} \tag{21}$$

where T= temperature in K (in our case, 300 K); A=-0.000612; B=2.43; C=0.0577; D=0.43; and T_c=647.1 K.

These values represent an average for many woods and serve as a guideline only. Then the variation of wood modulus with relative humidity in our case, as expressed by Eq. (22), can be obtained by substituting Eqs. (20) and (21) into Eq. (19):

$$\frac{E}{E_0} = 1 - 1.09\left[AT\left(1-\frac{T}{T_c}\right)^{B} ln(1-h)\right]^{CT^{D}} \tag{22}$$

Fig. 9a shows the variation of E with h for the three layers considered in the calculation. The Young's modulus increases very fast with the initial stages of humidity decrease (from 1 to 0.9), after which the increase is much more gradual. The corresponding stresses in the three layers as a function of h are given in Fig. 9b.The incorporation of the humidity dependence of E indicates that the linear dependence of the stresses on humidity is replaced by a non-linear dependence. The stresses are significantly reduced at high humidity but approach the values predicted by the simple analysis of Fig. 8e as the humidity approaches zero.

3.5. Robust bending actuation of cone scales induced by hydration

In order to evaluate the robustness of the actuation of the pine cone with the ingenious design described above, the actuation force was tested in successive cycles using the experimental setup presented in Fig. 10a. The base part of the scale is fixed onto ae clamp with the tip part contacted to the load cell. The actuation force is generated by immersing the cone scale in hot water, which serves to accelerate the actuation. The actuation force was recorded for approximately 2 h until it stabilized. After each test, the specimen was dehydrated for 24 h in a desiccator, until it retracted to its original position, and then another cycle of force test was conducted. The actuation force for a representative specimen tested for three such cycles is shown in Fig. 10b. Three previously unreported aspects can be seen:

First, since the hygroscopic actuation is based on the diffusion of water in the pine cone tissue, as the tissue is immersed in water the actuation force also grows in an approximate logarithmic manner, reaching a plateau when the tissue is fully hydrated.

Second, the maximum actuation force generated by the hydration-induced bending of the pine cone scale is very impressive at ~12N in these samples; for other samples shown in Fig. S5, the measured activation force actually reached as high as 16 N.

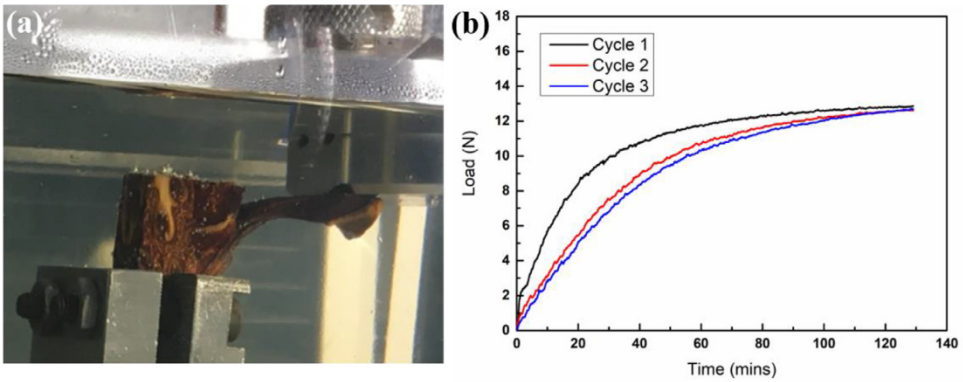

Fig. 10. Actuation force test. (a) Experimental setup for the actuation force test. (b) The actuation force generated by the hygroscopic movement of one pine cone scale in three successive cycles of hydration and dehydration.

Since the average weight of an isolated scale of the cone species that we investigated is a mere ~1g, such bending actuation of a cone scale can generate an actuation force more than 1000 times of its own weight, which demonstrates the efficiency of its actuation mechanism [40].

Third, which is also the most important discovery here, is that there is no significant drop in the maximum actuation force when the cone scale is subjected to several cycles of hydration and dehydration. This highly reversible deformation is attributed to the intricate gradient design described in Section 3.4. With the presence of the graded porosity, the stress concentration between the sclerenchyma and sclereids is substantially reduced, which significantly increases the interfacial toughness, making the cone scale a very robust and durable actuation design.

4. Summary and conclusions

Many plants rely on passive movement to disperse the seeds or improve their dispersal. The hydration-induced bending of pine cone is one of the best-known examples. Previous investigations showed that this highly reversible and humidity-driven deformation is due to the different cellulose microfibril angles with the longitudinal scale axis in a bi-layered structure arrangement, causing differences in the directional swelling in the two layers. The mismatch of the swelling strain generates the bending movement in a manner akin to bi-layer thermostats.

We found that, in addition this, porosity gradients in the tissue of the pine cone scale, first observed by Song and Lee [20] and Correa et al. [21], also contribute significantly to the bending deformation and to the decrease in the internal stresses generated by such bending. The contribution of this porosity gradient to the hygroscopic deformation is validated using simulations with synthesized bi-layer hydrogels that we produced with distinct porosities in the two layers. Moreover, the porous sclereid cells between sclerenchyma and dense sclereid act as a cushion layer to enhance the mechanical performance for the cone scales. This is corroborated by quantitative analysis based on a tri-layer model, which captures the essential characteristics of the graded porous design, and reveals that the stress concentration generated at the interface between sclerenchyma and sclereids during the hydration-induced bending can be substantially reduced. This results in an increased interfacial toughness and significantly improves the reversibility and robustness of the bending actuation for the cone scales.

The combination of different microfibril angles for the two layers comprising the pine cone (sclereids and sclerenchyma) coupled with the porosity gradient confer the pine cone with a highly efficient actuation mechanism to generate the effective reversible deformation stimulated by the environmental variation, which effectively improves the seed dispersal range which is important for the reproduction of pines. Additionally, measurements on separated bundles of sclerenchyma fibers and a sclereid layer show that they also bend independently, providing further synergy for the robustness of the scales. Our study may provide inspiration for the development of more efficient smart responsive materials with simpler simulative strategy and better biocompatibility.

One final note - we expected that when cone scales open, seeds can be released and then the cones cease to perform a useful function, fall to the ground, and decompose. However, when we pick up pine cones along the Torrey Pine Road, we find that some of them, principally the ones that are relatively fresh but also some old ones, still contain seeds inside. A representative example is shown in Fig. S6. Although the cone scales are open, several seeds are still trapped inside. Successive cycles of opening and closing can release these seeds and effectively increase their chance of survival. We believe that these cones could go through additional complete rounds of opening-closure process, given the seasonal weather at that time. This suggests that all the seeds are not completely released at once and that the cones have to go through several cycles of reversible opening and closing to release most seeds at a favorable timing. As we demonstrate in this work, the enhanced interfacial toughness of the graded layered structure inside the cone scales can ensure the robust reversible opening of pine cone and enable them to release as many seeds as possible, since this is important for the survival of plant species. Indeed, the additional toughness and reversibility provided by the gradient structure appears to enable the pine cones to release the seeds over a considerable period of time.

Declaration of Competing Interest

None

Acknowledgments

This work was supported by the Multidisciplinary University Research Initiative to University of California Riverside, funded by the Air Force Office of Scientific Research (AFOSR-FA9550-15-1-0009), with subcontracts to UC San Diego and UC Berkeley. We appreciate the significant intellectual contribution by Prof. Vlado Lubarda on the quantitative analysis of the tri-layer model. Fabio da Costa Garcia Filho performed the porosity measurements and confirmed the quantitative analysis through independent calculations; his help was invaluable. Alex Li kindly calculated the stresses for variable Young moduli. We appreciate the help from Audrey Velasco-Hogan on the preparation of polished specimens and their photographing. We acknowledge Eric Bushong for his help with the micro-CT, on a facility that is funded by National Institutes of Health Grant No. P41GM103412 to Mark H. Ellisman. We appreciate the contribution from the labs of Shengqiang Cai and Renkun Chen: Qiguang He, Zhijian Wang and Qingyang Wang help us on the synthesis of hydrogels. Qingyang Wang and Shuang Cui also helped us on the moisture sorption isotherm experiment. We are also grateful to Yufei Ding for his contribution to the early investigation of this work.

Supplementary materials

Supplementary material associated with this article can be found, in the online version, at doi:10.1016/j.actbio.2021.04.049.

References

[1] M.A. Meyers, P.Y. Chen, Biological materials science: biological materials, Bioinspired Materials, and Biomaterials, 1st ed., Cambridge University Press, Cambridge, 2014.
[2] R. Elbaum, Y. Abraham, Insights into the microstructures of hygroscopic movement in plant seed dispersal, Plant Sci. 223 (2014) 124–133.
[3] J. Teyssier, S.V. Saenko, D. van der Marel, M.C. Milinkovitch, Photonic crystals cause active colour change in chameleons, Nat. Commun. 6 (1) (2015) 6368.
[4] G.K. Szulgit, R.E. Shadwick, Dynamic mechanical characterization of a mutable collagenous tissue: response of sea cucumber dermis to cell Lysis and dermal extracts, J. Exp. Biol. 203 (10) (2000) 1539–1550.
[5] H. Hofhuis, A. Hay, Explosive seed dispersal, New Phytol. 216 (2) (2017) 339–342.
[6] J. Dumais, Y. Forterre, Vegetable dynamics": the role of water in plant movements, Annu. Rev. Fluid Mech. 44 (1) (2012) 453–478.
[7] H. Quan, D. Kisailus, M.A. Meyers, Hydration-induced reversible deformation of biological materials, Nat. Rev. Mater. 5 (2020).
[8] R. Elbaum, L. Zaltzman, I. Burgert, P. Fratzl, The Role of wheat awns in the seed dispersal unit, Science 316 (5826) (2007) 884–886.
[9] D. Evangelista, S. Hotton, J. Dumais, The mechanics of explosive dispersal and self-burial in the seeds of the filaree, Erodium cicutarium (Geraniaceae), J. Exp. Biol. 214 (4) (2011) 521–529.
[10] Y. Abraham, C. Tamburu, E. Klein, J.W.C. Dunlop, P. Fratzl, U. Raviv, R. Elbaum, Tilted cellulose arrangement as a novel mechanism for hygroscopic coiling in the stork's bill awn, J. R. Soc. Interface 9 (69) (2012) 640–647.
[11] M.J. Harrington, K. Razghandi, F. Ditsch, L. Guiducci, M. Rueggeberg, J.W.C. Dunlop, P. Fratzl, C. Neinhuis, I. Burgert, Origami-like unfolding of hydro-actuated ice plant seed capsules, Nat. Commun. 2 (1) (2011) 337.

[12] W.M. Harlow, W.A. Côté, A.C. Day, The opening mechanism of pine cone scales, J. For. 62 (8) (1964) 538–540.
[13] C. Dawson, J.F.V. Vincent, A.-M. Rocca, How pine cones open, Nature 390 (6661) (1997) 668–668.
[14] E. Reyssat, L. Mahadevan, Hygromorphs: from pine cones to biomimetic bilayers, J. R. Soc. Interface 6 (39) (2009) 951–957.
[15] S. Poppinga, N. Nestle, A. Šandor, B. Reible, T. Masselter, B. Bruchmann, T. Speck, Hygroscopic motions of fossil conifer cones, Sci. Rep. 7 (1) (2017) 40302.
[16] K. Song, E. Yeom, S.-J. Seo, K. Kim, H. Kim, J.-H. Lim, S. Joon Lee, Journey of water in pine cones, Sci. Rep. 5 (1) (2015) 9963.
[17] K. Song, S.J. Lee, Pine cone scale-inspired motile origami, NPG Asia Mater. 9 (6) (2017) e389–e389.
[18] W.L. Kilmer, On growing pine cones and other Fibonacci fruits— McCulloch's localized algorithm, Math. Biosci. 11 (1) (1971) 53–57.
[19] J.-Y. Sun, X. Zhao, W.R.K. Illeperuma, O. Chaudhuri, K.H. Oh, D.J. Mooney, J.J. Vlassak, Z. Suo, Highly stretchable and tough hydrogels, Nature 489 (7414) (2012) 133–136.
[20] B. Sun, Z. Wang, Q. He, W. Fan, S. Cai, Porous double network gels with high toughness, high stretchability and fast solvent-absorption, Soft Matter 13 (38) (2017) 6852–6857.
[21] P. Fratzl, R. Elbaum, I. Burgert, Cellulose fibrils direct plant organ movements, Faraday Discuss. 139 (2008) 275–282.
[22] S. Zabler, O. Paris, I. Burgert, P. Fratzl, Moisture changes in the plant cell wall force cellulose crystallites to deform, J. Struct. Biol. 171 (2) (2010) 133–141.
[23] D. Borowska-Wykręt, A. Rypień, M. Dulski, M. Grelowski, R. Wrzalik, D. Kwiatkowska, Gradient of structural traits drives hygroscopic movements of scarious bracts surrounding Helichrysum bracteatum capitulum, Ann. Bot. 119 (8) (2017) 1365–1383.
[24] D. Correa, S. Poppinga, M.D. Mylo, A.S. Westermeier, B. Bruchmann, A. Menges, T. Speck, 4D pine scale: biomimetic 4D printed autonomous scale and flap structures capable of multi-phase movement, Philos. Trans. R. Soc. A 378 (2167) (2020) 20190445.
[25] E.T. Engelund, L.G. Thygesen, S. Svensson, C.A.S. Hill, A critical discussion of the physics of wood–water interactions, Wood Sci. Technol. 47 (1) (2013) 141–161.
[26] C. Skaar, Wood-water relationships: the chemistry of solid wood, Am. Chem. Soc. (1984) 127–172.
[27] S.L. Zelinka, S.V. Glass, E.E. Thybring, Evaluation of previous measurements of water vapor sorption in wood at multiple temperatures, Wood Sci. Technol. 54 (4) (2020) 769–786.
[28] E.E. Thybring, S.V. Glass, S.L. Zelinka, Kinetics of water vapor sorption in wood cell walls: state of the art and research needs, Forests 10 (8) (2019) 704.
[29] L. Li, C. Ortiz, Biological materials: a natural 3D interconnected laminated composite with enhanced damage resistance, Adv. Funct. Mater. 25 (23) (2015) 3445–3445.
[30] H. Quan, W. Yang, Z. Tang, R.O. Ritchie, M.A. Meyers, Active defense mechanisms of thorny catfish, Mater. Today 38 (2020) 35–48.
[31] M. Tadayon, S. Amini, A. Masic, A. Miserez, The mantis shrimp saddle: a biological spring combining stiffness and flexibility, Adv. Funct. Mater. 25 (41) (2015) 6437–6447.
[32] T. Watanabe, Y. Imamura, Y. Hosaka, H. Ueda, K. Takehana, Graded arrangement of collagen fibrils in the equine superficial digital flexor tendon, Connect. Tissue Res. 48 (6) (2007) 332–337.
[33] A.R. Studart, Biological and bioinspired composites with spatially tunable heterogeneous architectures, Adv. Funct. Mater. 23 (36) (2013) 4423–4436.
[34] S. Suresh, Graded materials for resistance to contact deformation and damage, Science 292 (5526) (2001) 2447–2451.
[35] Z. Liu, M.A. Meyers, Z. Zhang, R.O. Ritchie, Functional gradients and heterogeneities in biological materials: design principles, functions, and bioinspired applications, Prog. Mater. Sci. 88 (2017) 467–498.
[36] S. Timoshenko, Analysis of bi-metal thermostats, J. Opt. Soc. Am. 11 (3) (1925) 233–255.
[37] C.C. Gerhards, Effect of moisture content and temperature on the mechanical properties of wood: an analysis of immediate effects, Wood Fiber 14 (1) (1982) 1–36.
[38] S. V. Glass, S. L. Zelinka, J. A. Johnson, Investigation of historic equilibrium moisture content data from the Forest Products Laboratory. General Technical Report FPL–GTR–229. Madison, WI: U.S. Department of Agriculture, Forest Service, Forest Products Laboratory. (2014).
[39] S.V. Glass, S.L. Zelinka, Centennial (Ed.), Moisture Relations and Physical Properties of Wood, Wood Handbook: Wood as an Engineering Material: Chapter 4, U.S. Dept. of Agriculture, Forest Service, Forest Products Laboratory, Madison, WI, 2010 General Technical report FPL; GTR-190p. 4.1-4.19.
[40] M. Mirvakili, I.W. Hunter, Artificial muscles: mechanisms, applications, and challenges, Adv. Mater. 30 (6) (2018) 1704407.